## PAPER

Check for updates

# Sn-encapsulated N-doped porous carbon fibers for enhancing lithium-ion battery performance†

Zhilong Xu, Lei Fan,* Xiangying Ni, Jie Han [ID] * and Rong Guo [ID]

Tin (Sn) has wide prospects in applications as an anode electrode material for Li-ion batteries, due to its high theoretical specific capacity. However, the large volume expansion of Sn during the charge–discharge process causes a performance reduction of lithium-ion batteries (LIBs). Here, Sn encapsulated N-doped porous carbon fibers (Sn/NPCFs) were synthesized through an electrospinning method with a pyrolysis process. This structure was beneficial for the lithium ion/electron diffusion and buffered the large volume change. By adjusting the amount of Sn, the hybrid carbon fibers with different Sn/carbon ratios could be prepared, and the morphology, composition and properties of the Sn/NPCFs were characterized systematically. The results indicated that the Sn/NPCFs with a Sn-precursor/polymer weight ratio at 0.5 : 1 showed the best cycling stability and specific capacity, preserving the specific capacity of 400 mA h g$^{-1}$ at the current density of 500 mA g$^{-1}$ even after 100 cycles.

## Introduction

Lithium-ion batteries, due to their high capacity and long cycling life, have been presented as a meaningful prospect for applications in a variety of fields, including portable electronic devices, grid energy storage and electric vehicles.[1] Currently, many anode materials have been developed, including graphite,[2–4] silicon,[5] tin (Sn)[6] and ferroferric oxide.[7] Among these materials, Sn, as a transition metal with high theoretical specific capacity, is widely used as an anode electrode for LIBs.[8] However, Sn-based materials still have serious defects. One of the most urgent problems is volume expansion during the charge and discharge process, because the large volume expansion of Sn during the lithiation/delithiation process usually causes a performance reduction of lithium-ion batteries (LIBs).[9–11] To address this drawback, two strategies have been proposed: one is to prepare small-sized Sn particles to reduce the absolute volume;[12–14] and the other is to design a hollow structure in electrodes to provide the space for volume expansion.[15–18] For example, some core/shell, yolk–shell, and multi-layer structure Sn/carbon materials have been reported.[19–22] Nevertheless, when they are used as electrode materials, it is often necessary to add binders and conductors to improve the electron transport ability, even though they make no contribution to the improvement of capacity. Considering this, one-dimensional (1D) nanomaterials (for instance: nanowires, nanotubes and nanofibers) may give an opportunity to improve the electrochemical performance and battery lifetime, due to their special electrical and physical properties.[23–28]

Electrospinning is a common method to prepare 1D polymer fibers.[29] Polyacrylonitrile (PAN) is the most widely used polymer in electrospinning, which is also used as a carbon fiber precursor.[30] Dong *et al.*[31] grew ZIF-67 nanocrystals on PAN/2-methylimidazole nanofibers and carbonized to obtain graded porous carbon nanofibers/$Co_3O_4$ composite nanomaterials, which showed excellent electrochemical performance. As to Sn/carbon materials, although some pore structures could be formed during the carbonization process, their pore size is generally small and could not provide sufficient space for the expansion of metal tin. Therefore, it is necessary to design a more reasonable Sn-based anode material to control the size and void volume.

In this paper, we reported the synthesis of Sn/NPCFs by electrospinning method with a carbonization process. The porous structure of Sn/NPCFs could promote the diffusion of lithium ions into their inward structure and transport of electrons during the charge/discharge process and provide space for volume expansion of Sn, which is benefit for the improvement of lithium-ion battery performance. Form the results we can find that the addition of Sn can increase the specific capacity of the anode materials, it still reveals a good cycle stability.

## Experimental

### Materials

Ethanol, *N*,*N*-dimethylformamide, sodium hydroxide, urea and ammonia water were sold by Sinopharm Chemical Reagent Co. Ltd. (China). Polyacrylonitrile (PAN), polyvinylpyrrolidone (PVP) and potassium stannate trihydrate ($K_2SnO_3$) were obtained

*School of Chemistry and Chemical Engineering, Yangzhou University, Yangzhou, Jiangsu, 225002, P. R. China. E-mail: fanlei@yzu.edu.cn; hanjie@yzu.edu.cn*

† Electronic supplementary information (ESI) available: Additional TEM, SEM, charge and discharge curves of NPCFS. See DOI: 10.1039/c8ra10201e

from Shanghai Aladdin Biochemical Technology Co., Ltd. (China). Tetraethyl orthosilicate (TEOS) was sold by Sigma Aldrich (Shanghai) Trading Co., Ltd. The electrolyte solution with 1 M $LiPF_6$/ethylene carbonate (EC)/diethyl carbonate (DMC)/ethyl methyl carbonate (EMC) (1 : 1 : 1 by volume) were purchased from Guangzhou Tinci Materials Technology Co., Ltd. (China).

### Synthesis of $SiO_2$

$SiO_2$ nanospheres were synthesized according to the literature.[32] First, 3.15 mL of ammonia water was added to a mixed solution of 74 mL of absolute ethanol and 10 mL of deionized water, and then stirred for 1 h. Next, 6 mL TEOS was added to the above mixture and kept stirring for another 3 h at 50 °C. Finally, the $SiO_2$ nanoparticles were separated by centrifugation, washed and dried for further use.

### Synthesis of $SnO_2/SiO_2$

$SnO_2/SiO_2$ nanospheres were synthesized according to the literature.[33] 20 mg $SiO_2$, 50 mg $K_2SnO_3$, 450 mg $CO(NH_2)_2$ and 5.62 mL deionized water were added to a 25 mL beaker. The sample was homogenized by sonication with the addition of 9.38 mL ethanol. Next, the mixture was transferred into a Teflon-lined autoclave, reacted at 170 °C for 1 h. After cooled to room temperature, the product was gathered by centrifugation (6000 rpm, 8 min), then washed with distilled water and ethanol several times. Then black powders of $SnO_2/SiO_2$ were obtained after dried at 60 °C overnight.

### Synthesis of $SnO_2/SiO_2/PVP/PAN$ fibers

A certain amount of $SnO_2/SiO_2$ was dispersed in 2.67 mL DMF. After the treatment with ultrasound for 1 h, 0.76 g PVP in 2.67 mL DMF was added slowly. Next, 0.76 g PAN was added into the above dispersion and stirred for 4–5 h. Then the above mixture was poured into a 10 mL syringe with an inner diameter of 6 mm. In the electrospinning process, the applied voltage was controlled at 15 kV, the distance was 15 cm with the flow rate of 0.2 mm $min^{-1}$.

### Synthesis of Sn/NPCFs fibers

The above obtained fibers were then stabilized in $N_2$ atmosphere at 250 °C for 1 h at 1 °C $min^{-1}$, and then calcined at 800 °C for 2 h at 5 °C $min^{-1}$. After that, the fibers were soaked in 1 M NaOH for 2 h, washed with deionized water until pH = 7, and finally dried at 65 °C. The synthesis of carbon fibers without Sn were according to the literature.[34] By controlling the different mass ratios of $SnO_2/SiO_2$ and PAN/PVP ($SnO_2/SiO_2$ : PAN/PVP = 0.2 : 1, 0.5 : 1, 1 : 1), a series of Sn/NPCFs could be obtained and denoted as Sn/NPCFs-0.2, Sn/NPCFs-0.5, Sn/NPCFs-1, respectively.

### Electrochemical tests

We punched the carbon material into a circular shape with a diameter of 16 mm. Since the self-supporting structure the carbon fiber can be directly used as a anode electrode material without adding any binder. The CR2032 coin-type cells were assembled in argon-filled glove box. Cyclic voltammograms (CVs) was performed using an electrochemical workstation (VMP3, Bio-logic, France) at a scan rate of 0.1 mV $s^{-1}$ between 0.01 and 3.0 V. Galvanostatic charge and discharge cycling of the cells were carried out using a battery test system (CT-3008W, Xinwei, China) and the current densities were between 0.01 and 3 V (vs. $Li^+/Li$) at the current density of 0.5 A $g^{-1}$. The thickness of the Sn/NPCFs electrode is 200 ± 20 μm and the average area mass loading of the active materials on the Sn/NPCFs electrodes is 1.5 ± 0.15 mg $cm^{-2}$.

### Characterization

The morphology of the as-obtained Sn/NPCFs was obtained with scanning electron microscopy (SEM, Zeiss 55), transmission electron microscopy (TEM, JEM-2100), high-resolution TEM (HRTEM, Tecnai G2 F30 S-Twin). The crystal structure of the material was measured by X-ray diffraction (XRD, D8 Advance). The elemental valence was measured by X-ray photoelectron spectroscopy (XPS, ESCALAB 250Xi). The thermal stability of materials was inspected by thermogravimetric analysis (TGA, Pyris 1 TGA) from room temperature to 800 °C in an oxygen atmosphere using a temperature ramp of 5°C $min^{-1}$. The specific surface area and pore size distribution were studied by the gas sorption analysis instrument (Beishide, 3H-2000PS2).

## Results and discussion

The synthetic steps are displayed in Scheme 1. First, the average size of the uniform $SiO_2$ nanoparticles (Fig. S1†) was 200 nm.[32] Next, $SiO_2/SnO_2$ nanoparticles were obtained through the hydrothermally reaction between $SiO_2$, $K_2SnO_3$ and $CO(NH_2)_2$. Fig. 1a confirmed that $SnO_2$ evenly distributed on the surfaces of $SiO_2$ nanoparticles. It can be seen from Fig. S2† that $SnO_2$ was uniformly scattered on the external of $SiO_2$, and the energy dispersive X-ray spectroscopic (EDS) elemental analysis and EDS mapping had been used, and the results were also confirmed to be consistent with Fig. S2b–f.† After electrospinning, $SiO_2/SnO_2$ polymer fibers could be obtained, as displayed in Fig. 1b. Through the carbonization and NaOH etching, $SnO_2$ was converted into Sn, yield of Sn/NPCFs (Fig. 1b). The SEM image of Sn/NPCFs-0.5, shown in Fig. 1c, indicated that the diameter of the carbon fibers was about 1.3 μm. Moreover, the obvious pores in the carbon fibers could be surveyed from the TEM image (Fig. 1d), and the number of pores in the fiber was increased with the $SiO_2/SnO_2$ content (Fig. S3 a and b†). The TEM image of Sn/NPCFs-0.5 clearly
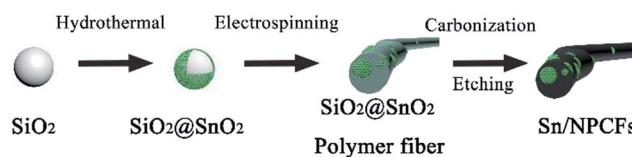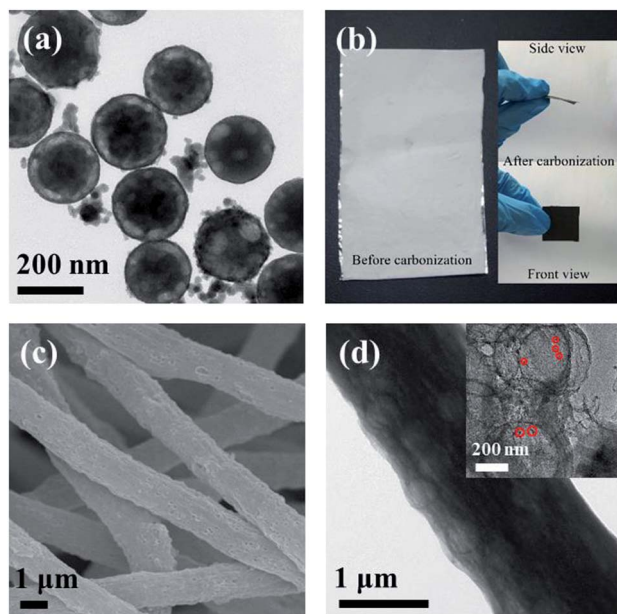


**Scheme 1** The fabrication process of the Sn/NPCFs.

Fig. 1 (a) TEM image of SiO$_2$/SnO$_2$, (b) the image of monolayer fiber before and after carbonization, (c) SEM image of Sn/NPCFs-0.5, (d) TEM image of Sn/NPCFs-0.5.

indicated that the Sn nanoparticles (in red circles) were in the porous carbon fibers (Fig. 1d illustration). Similarly, Sn nanoparticles could also be found in Sn/NPCFs-0.2 and Sn/NPCFs-1, and the amount of Sn nanoparticles in fibers increased with the mass ratio of SiO$_2$/SnO$_2$ increasing (Fig. S4†). The Fig. 2a exhibits the hollow interior explicitly. The composition of Sn/NPCFs could be further confirmed according to the elemental mapping. The EDS mapping of C, N, and Sn elements within a single hollow space was behave in Fig. 2b–e, indicating the elements distributed in the shell evenly. It was worth emphasizing that Sn were uniformly attached to the inner wall of the hole after carbonization. This porous structure is conducive to the transfer of lithium ions and provides the channels for the transmission of lithium ions into the inner part of the electrode material.

The crystal structures of Sn/NPCFs-0.2, Sn/NPCFs-0.5 and Sn/NPCFs-1 were determined through the XRD measurements and the results were presented in Fig. 3a. The typical peaks for Sn

could be evidenced (JCPDS no: 86-2265). The content of Sn was then analyzed by TGA.[35] With the increase of the SnO$_2$/SiO$_2$ ratio, the remaining amount of the Sn gradually increased from 18.6% to 24.1% (Fig. 3b). After 600 °C, the TGA curve has a slow upward trend, indicating that part of Sn was oxidized to SnO, and even oxidized to SnO$_2$, which could further prove the existence of Sn in the fibers. The specific surface area (SSA) of Sn/NPCFs was measured with the multipoint Brunauer–Emmett–Teller (BET) method, the porous structure was calculated by using the Barrett–Joyner–Halenda (BJH) method. The nitrogen adsorption–desorption isotherm was shown in Fig. S5† and in a typical type IV curve. The SSAs of the NPCFs, Sn/NPCFs-0.2, Sn/NPCFs-0.5 and Sn/NPCFs-1 were 40.99 m$^2$ g$^{-1}$, 43.95 m$^2$ g$^{-1}$, 93.55 m$^2$ g$^{-1}$ and 155.4 m$^2$ g$^{-1}$, respectively. Meanwhile, the pore sizes were about 3.30 nm, 3.97 nm, 4.05 nm, 4.03 nm, respectively. It was easy to confirm that the mass ratio of SiO$_2$/SnO$_2$ was the main impact factor for the specific surface area of the material. The related data had been arranged in the Table S1.† From the Table S1,† it can be found that the Sn/NPCFs-0.5 has the biggest volume of pores, which was in favor of the transfer of lithium ions.

The XPS further confirmed that Sn/NPCFs-0.5 comprised the C, N, O, and Sn, respectively (Fig. 4a). This result was consistent with the EDS analysis (Fig. S6†). As denoted in Fig. 4a, the peaks appeared at 531 eV, 484 eV, 400 eV, and 284 eV corresponding to O 1s, Sn 3d, N 1s, and C 1s peaks originated from Sn and PAN were observed. The C 1s spectrum of Sn/NPCFs-0.5 was given in Fig. 4b. The peaks at 284.8, 286.0, 287.0, and 288.2 eV were ascribed to the binding energy of graphitized carbon, C–N group, C=N group and O=C–N group bonds, respectively.[36] The N 1s spectra of Sn/NPCFs-0.5 (Fig. 4c) could be analyzed into pyridine N (398.3 eV), pyrrole N (400.1 eV), quaternary N (401.2 eV) and oxidized N (402.7 eV).[37] More open channels and active sites were created by pyridinic N and pyrrolic N, which were in favor for the Li$^+$ insertion.[38] The Sn 3d spectra of Sn/NPCFs-0.5 (Fig. 4d) was put down to Sn 3d$_{5/2}$ (484.3 eV) and Sn 3d$_{3/2}$ (492.6 eV).[39] The spin energy separation between the two peaks is 8.5 eV, which verified the existence of Sn.[40] In summary, the Sn/carbon fiber porous composite material was successfully framed, and the Sn/NPCFs electrode was electrochemically test.

The electrochemical reactivity of Sn/NPCFs-0.5 was evaluated by CVs at a sweep speed of 0.1 mV s$^{-1}$ (Fig. 5a). The CV curves demonstrated that a broad irreversible peak occurs at the first cycle, owing to the Li$^+$ formation during the migration process
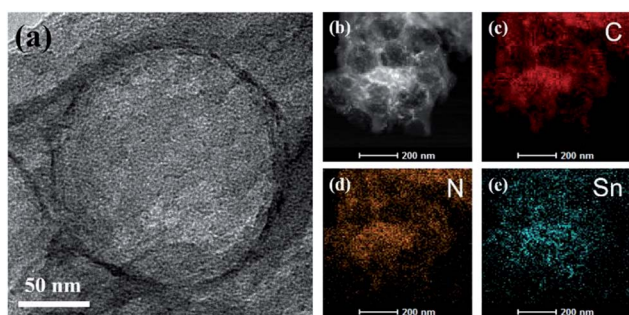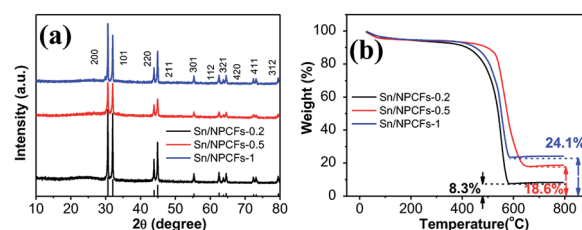


Fig. 2 (a) HRTEM image of Sn/NPCFs-0.5. (b) HAADF-STEM image of Sn/NPCFs-0.5 and (c and d) EDS mappings of (c) C, (d) N and (e) Sn from Sn/NPCFs-0.5 particle given in panel (b).



Fig. 3 (a) XRD pattern of Sn/NPCFs-0.2, Sn/NPCFs-0.5 and Sn/NPCFs-1; (b) TGA of Sn/NPCFs-0.2, Sn/NPCcFs-0.5 and Sn/NPCFs-1.
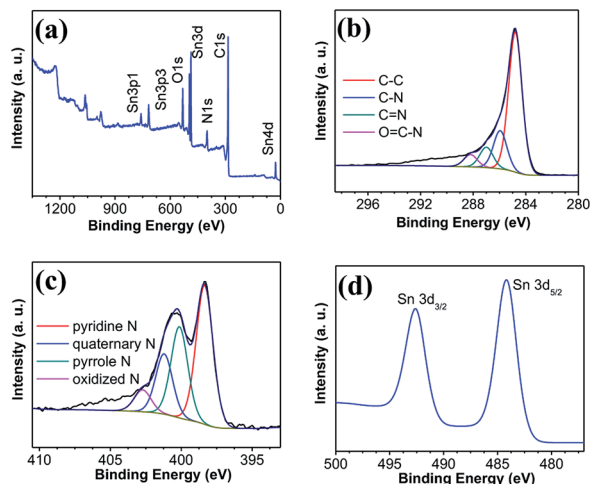
**Fig. 4** XPS spectrum of Sn/NPCFs-0.5; (a) the survey, (b) C 1s, (c) N 1s, (d) Sn 3d.
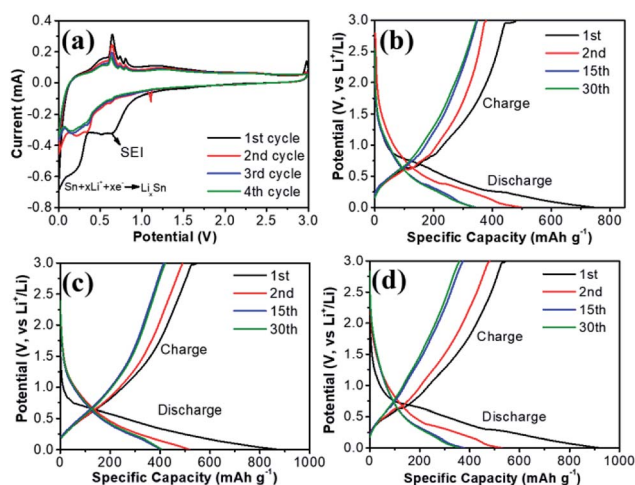


**Fig. 5** (a) Cyclic voltammograms (CVs) of Sn/NPCFs-0.5 at a scan rate of 0.1 mVs$^{-1}$, voltage profiles of (b) Sn/NPCFs-0.2, (c) Sn/NPCFs-0.5, (d) Sn/NPCFs-1 at 0.5 A g$^{-1}$.

and the reaction between the anode electrode and the electrolyte leading to the solid electrolyte interface (SEI) film.[41] The formation of SEI film leaded to the difference between the first and the second cathodic scans. During the cathodic sweep, the reduction peaks located at 0.21, 0.34, and 0.62 V were intrinsically attributed to the lithiation into Sn to form Li$_x$Sn alloy.[41,42] During the anodic scan, the oxidation peaks at 0.53 V, 0.67 V and 0.80 V were corresponding to the delithiation reaction of Li$_x$Sn alloy.[43] The good cycle stability of Sn/NPCFs is evidenced by the overlap of the CV curves after the second cycle.[44] In the CV curve, there is a significant reduction peak at 1.1 V in the second pass, indicating that lithium is inserted into the carbon fiber matrix.[45,46] Simultaneously, it could also be proved by a wide small oxidation peak at 1.3 V. Furthermore, an oxidation peak was appeared at about 2.95 V in the first scan, which disappears in the subsequent cycle. This is due to the disintegration of the SEI film.[40,47,48] The charge–discharge voltage profiles of the pure

NPCFs, Sn/NPCFs-0.2, Sn/NPCFs-0.5 and Sn/NPCFs-1 were shown in Fig. 5b–d and S3.† The coulombic efficiency (CE) of the initial cycle of Sn/NPCFs-0.2, Sn/NPCFs-0.5, Sn/NPCFs-1 were 65.5%, 62.9% and 59.6%, respectively. The CE difference of each Sn/NPCFs for initial cycle was not obvious. But the CE of Sn/NPCFs-0.5 for the subsequent cycles was 94.3%, which was higher than the CE of Sn/NPCFs-0.2 and Sn/NPCFs-1 (76.08% and 90.72%). In Fig. S7,† the charge and discharge capacity of NPCFs indicated that the porous N-doped carbon material had a positive effect on the capacity. It should be ascribed to the doped heteroatom (such as N) could enhance electrochemical reactivity and electron conductivity, as well as the performance of LIBs and supercapacitor with high energy and power density.[49,50] The NPCFs material increases the coulombic efficiency, but the specific capacity was still unsatisfactory. The heteroatoms in the carbon structure can increase the conductivity and capacity of the carbon-based material, thereby increasing the coulombic efficiency of the NPCFs. In Fig. 5b, the charge/discharge of first cycle capacity of Sn/NPCFs-0.2 were improved to 744, 481 mA h g$^{-1}$, respectively. By comparing the charge/discharge capacity data of Sn/NPCFs and NPCFs, it was found that the addition of Sn had a great improvement on the specific capacity of the material. The charge and discharge of the increased content of Sn were exhibited in Fig. 5c. The charge/discharge of second cycle of Sn/NPCFs-0.5 had a significant coulomb efficiency improvement over the first cycle. The irreversible capacity loss of Sn/NPCFs-0.5 was mainly caused by the first irreversible cycle, which agreed with the CV curves. After 4 cycles, the capacity of the electrode material was substantially not attenuated, and the specific capacity retention rate was 86%, which indicated that the stability of the electrode material was particularly good. Moreover, from the fourth cycle, the coulombic efficiency was almost 100%. In Fig. 5d, Sn/NPCFs-1 had no significant increase in specific capacity after thirty cycles of charging and discharging compared with Sn/NPCFs-0.5. The Sn/NPCFs-0.5 electrode delivered a lithium storage capacity of 375 mA h g$^{-1}$ after 30 cycles, better than previously reported Sn/graphene nanocomposite.[51] Without the Sn-encapsulated, NPCFs shows the worst specific capacity.

In order to study the cycling performance of materials, it was subjected to 100 cycles of charge and discharge. The discharge capacity of the Sn/NPCFs-0.2 electrode was significantly higher than that of the NPCFs after 100 cycles. Nevertheless, the Sn/NPCFs-0.5 electrode still hold comparatively high discharge capacity of 400 mA h g$^{-1}$. The second cycle retains 82.1% of the first (Fig. 6a). In addition, the discharge capacity of the Sn/NPCFs-1 was 377 mA h g$^{-1}$ ($\approx$70.9% preservation of the second cycle). The carbon cycle stability was good, but the specific capacity was low. With the increase of Sn, the specific capacity had increased. Once the content of Sn was too much, the electrode cycle stability and specific capacity were not significantly improved. Fig. 6b shows the rate performance of Sn/NPCFs-0.5 when it cycles at different rates between 0.05 A g$^{-1}$ and 2 A g$^{-1}$. When the current density reverts to 0.1 A g$^{-1}$ again, the specific capacity reached 639 mA h g$^{-1}$ that was 85% of the original one. It demonstrated the good cycle stability and specific capacity retention. The cycle performance and capacity of Sn/carbon nanomaterials reported
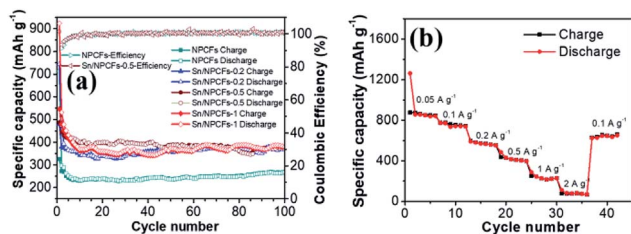
**Fig. 6** (a) Cycling performance of different electrode materials at 0.5 A g$^{-1}$, (b) rate performance of Sn/NPCFs-0.5.

in previous works had been compared with the Sn/NPCFs in Table S2.† Our results indicated certain advantages at low and medium current density.

Electrochemical impedance spectroscopy (EIS) was used to analyze the difference between Sn/NPCFs-0.5 and other Sn/NPCFs. Fig. S8† shows the impedance of Sn/NPCFs-0.5 on new coin cells on the basis of EIS. The frequency range was set between 100 kHz and 10 mHz with an AC amplitude of 10 mV. It can be seen that the four impedance spectra have similar features. From Fig. S8,† it was apparent that Sn/NPCFs-0.5 has a smaller semicircular arc, indicating that the charge transfer impedance ($R_{ct}$) of Sn/NPCFs-0.5 is the smallest. According to the equivalent circuit, the $R_{ct}$ of Sn/NPCFs-0.5 is 133.5 Ω, which is smaller than the others ($R_{ct}$-NPCFs = 235.2 Ω, $R_{ct}$-Sn/NPCFs-0.2 = 160.3 Ω, $R_{ct}$-Sn/NPCFs-1 = 140.3 Ω). At the same time, the faster rising linear tail of the low-frequency region indicated that Sn/NPCFs-0.5 has the smallest lithium ion diffusion impedance ($R_e$).

To further understand the electrochemical performance of Sn/NPCFs-0.5, the electrode changes were observed after 5 cycles of charge and discharge at 0.5 A g$^{-1}$. According to the SEM images, the formation of the SEI film on the electrode after several charge and discharge cycles had been confirmed (Fig. S9a and b†). It can be clearly seen from Fig. S9c† that the composite anode still retains the original appearance of the fibers. Meanwhile, there are also Sn nanoparticles in the fiber pores (Fig. S9d†). This proved that all the Sn nanoparticles are uniformly locked in the pores of the carbon fiber, and the unique structure of the Sn/NPCFs can buffer the volume expansion of the electrode material, thereby ensuring the stability. The excellent electrochemical performance of the Sn/NPCFs-0.5 electrodes might be attributed to the following factors. Firstly, the holes on the surface are beneficial for the lithium ions and electrons transferring to the inner part. Secondly, the porous structure provides a buffer for the volume expansion of lithium-ion batteries during charge and discharge. Finally, the synergistic effect of Sn and carbon composites was embodied in that the specific capacity of Sn is high and the cycle stability of carbon is good.

## Conclusions

The Sn/NPCFs composite fiber was obtained by electrospinning method followed by carbonization process. The results express that the Sn/NPCFs-0.5 has the best cyclic stability and specific capacity. The average specific capacity is 400 mA h g$^{-1}$ at 500 mA h g$^{-1}$. Because of the high capacity and excellent cycle stability, the Sn/NPCFs composites are expected a promising anode material for lithium-ion batteries.

## Conflicts of interest

There are no conflicts to declare.

## Acknowledgements

## Notes and references

1 M. Armand and J. M. Tarascon, *Nature*, 2008, **451**, 652.
2 M. Chhowalla, H. S. Shin, G. Eda, L. J. Li, K. P. Loh and H. Zhang, *Nat. Chem.*, 2013, **5**, 263.
3 L. G. Bulusheva, S. G. Stolyarova, A. Chuvilin, Y. Shubin, I. P. Asanov, A. M. Sorokin, M. S. Mel'Gunov, S. Zhang, Y. Dong and X. Chen, *Nanotechnology*, 2018, **29**, 134001.
4 R. Tjandra, W. Liu, L. Lim and A. Yu, *Carbon*, 2018, **129**, 152.
5 K. Xiao, Q. Tang, Z. Liu, A. Hu, S. Zhang, W. Deng and X. Chen, *Ceram. Int.*, 2018, **44**, 3548.
6 N. Zhang, Y. Wang, M. Jia, Y. Liu, J. Xu, L. Jiao and F. Cheng, *Chem. Commun.*, 2018, **54**, 1205.
7 R. Zhao, X. Shen, Q. Wu, X. Zhang, W. Li, G. Gao, L. Zhu, L. Ni, G. Diao and M. Chen, *ACS Appl. Mater. Interfaces*, 2017, **241**, 391.
8 J. Hassoun, G. Derrien, S. Panero and B. Scrosati, *Adv. Mater.*, 2008, **20**, 3169.
9 J.-M. Tarascon and M. Armand, *Nature*, 2001, **414**, 359.
10 A. Sivashanmugam, T. P. Kumar, N. G. Renganathan, S. Gopukumar, M. Wohlfahrt-Mehrens and J. Garche, *J. Power Sources*, 2005, **144**, 197.
11 K. Ui, S. Kikuchi, Y. Kadoma, N. Kumagai and S. Ito, *J. Power Sources*, 2009, **189**, 224.
12 X. He, W. Pu, L. Wang, J. Ren, C. Jiang and C. Wan, *Solid State Ionics*, 2007, **178**, 833.
13 P. Limthongkul, H. Wang, E. Jud and Y.-M. Chiang, *J. Electrochem. Soc.*, 2002, **149**, A1237.
14 N. Li and C. R. Martin, *J. Electrochem. Soc.*, 2001, **148**, A164.
15 Y.-X. Yin, S. Xin, L.-J. Wan, C.-J. Li and Y.-G. Guo, *J. Nanosci. Nanotechnol.*, 2012, **12**, 2581.
16 H. Wu, G. Chan, J. W. Choi, I. Ryu, Y. Yao, M. T. McDowell, S. W. Lee, A. Jackson, Y. Yang and L. Hu, *Nat. Nanotechnol.*, 2012, **7**, 310.
17 Y.-D. Ko, J.-G. Kang, G.-H. Lee, J.-G. Park, K.-S. Park, Y.-H. Jin and D.-W. Kim, *Nanoscale*, 2011, **3**, 3371.

18 U. Lafont, S. Waichman, M. Valvo and E. Kelder, *J. Nanosci. Nanotechnol.*, 2010, **10**, 4273.

19 J. S. Chen and X. W. Lou, *Small*, 2013, **9**, 1877.

20 J. Qin, C. He, N. Zhao, Z. Wang, C. Shi, E.-Z. Liu and J. Li, *ACS Nano*, 2014, **8**, 1728.

21 C. Wang, Y. Li, Y.-S. Chui, Q.-H. Wu, X. Chen and W. Zhang, *Nanoscale*, 2013, **5**, 10599.

22 X. Zhou, L. Yu, X. Y. Yu and X. W. Lou, *Adv. Energy Mater.*, 2016, **6**, 1601177.

23 Z. Xie, J. Zhao and Y. Wang, *Electrochim. Acta*, 2015, **174**, 1023.

24 Y. Hu, Q.-R. Yang, J. Ma, S.-L. Chou, M. Zhu and Y. Li, *Electrochim. Acta*, 2015, **186**, 271.

25 Y. J. Hong and C. K. Yun, *Small*, 2015, **11**, 2157.

26 J.-C. Kim, G.-H. Lee and D.-W. Kim, *Electron. Mater. Lett.*, 2013, **9**, 775.

27 L. Hu, H. Wu, S. S. Hong, L. Cui, J. R. McDonough, S. Bohy and Y. Cui, *Chem. Commun.*, 2011, **47**, 367.

28 J. Ren, X. He, K. Wang and W. Pu, *Ionics*, 2010, **16**, 503.

29 Z.-a. Wang, N. Li, W.-y. Lu and W.-x. Chen, *Acta Polym. Sin.*, 2018, 755.

30 J. Namsaeng, W. Punyodom and P. Worajittiphon, *Chem. Eng. Sci.*, 2019, **193**, 230–242.

31 H. Wang, Y. Song, Y. Li, M. Wang, Q. Ma, W. Yu, D. Li, X. Dong, J. Wang and G. Liu, *RSC Adv.*, 2018, **8**, 30794.

32 B. J. Ji, Z. Qiao, I. Lee, M. Dahl, F. Zaera and Y. Yin, *Adv. Funct. Mater.*, 2012, **22**, 166.

33 X. W. Lou, C. Yuan and L. A. Archer, *Small*, 2007, **3**, 261.

34 L. Fan, L. Yang, X. Ni, J. Han, R. Guo and C. Zhang, *Carbon*, 2016, **107**, 629.

35 X. Li, X. Li, L. Fan, Z. Yu, B. Yan, D. Xiong, X. Song, S. Li, K. R. Adair, D. Li and X. Sun, *Appl. Surf. Sci.*, 2017, **412**, 170.

36 M. Wang, J. Han, Y. Hu and R. Guo, *RSC Adv.*, 2017, **7**, 15513.

37 F. Yang, Z. Zhang, K. Du, X. Zhao, W. Chen, Y. Lai and J. Li, *Carbon*, 2015, **91**, 88.

38 Y. Liu, N. Zhang, L. Jiao and J. Chen, *Adv. Mater.*, 2015, **27**, 6702.

39 S. Wang, Y. Fang, X. Wang and X. W. Lou, *Angew. Chem., Int. Ed.*, 2019, **58**, 760.

40 R. Dai, W. Sun and Y. Wang, *Electrochim. Acta*, 2016, **217**, 123.

41 Y. Xu, Q. Liu, Y. Zhu, Y. Liu, A. Langrock, M. R. Zachariah and C. Wang, *Nano Lett.*, 2013, **13**, 470.

42 Z. Zhu, S. Wang, J. Du, Q. Jin, T. Zhang, F. Cheng and J. Chen, *Nano Lett.*, 2014, **14**, 153.

43 J. L. Tirado, R. Santamaría, G. F. Ortiz, R. Menéndez, P. Lavela, J. M. Jiménez-Mateos, F. J. Gómez García, A. Concheso and R. Alcántara, *Carbon*, 2007, **45**, 1396.

44 B. Luo, T. Qiu, D. Ye, L. Wang and L. Zhi, *Nano Energy*, 2016, **22**, 232.

45 X. Huang, S. Cui, J. Chang, P. B. Hallac, C. R. Fell, Y. Luo, B. Metz, J. Jiang, P. T. Hurley and J. Chen, *Angew. Chem., Int. Ed.*, 2015, **54**, 1490.

46 Y. Xu, Q. Liu, Y. Zhu, Y. Liu, A. Langrock, M. R. Zachariah and C. Wang, *Nano Lett.*, 2013, **13**, 470.

47 Y. Zou and Y. Wang, *ACS Nano*, 2011, **5**, 8108.

48 B. Guo, J. Shu, K. Tang, Y. Bai, Z. Wang and L. Chen, *J. Power Sources*, 2008, **177**, 205.

49 C. Hu, L. Wang, Y. Zhao, M. Ye, Q. Chen, Z. Feng and L. Qu, *Nanoscale*, 2014, **6**, 8002.

50 Z. Li, Z. Xu, X. Tan, H. Wang, C. M. B. Holt, T. Stephenson, B. C. Olsen and D. Mitlin, *Energy Environ. Sci.*, 2013, **6**, 871.

51 G. Wang, B. Wang, X. Wang, J. Park, S. Dou, H. Ahn and K. Kim, *J. Mater. Chem.*, 2009, **19**, 8378.